For final published version see doi: 10.1109/TBME.2021.3109384

Electro-optical classification of pollen grains *via* microfluidics and machine learning

Michele D'Orazio,‡ Riccardo Reale,‡ Adele De Ninno, Maria A. Brighetti, Arianna Mencattini, Luca Businaro, Eugenio Martinelli, Paolo Bisegna, Alessandro Travaglini, and Federica Caselli*

***Abstract*— *Objective:* In aerobiological monitoring and agriculture there is a pressing need for accurate, label-free and automated analysis of pollen grains, in order to reduce the cost, workload and possible errors associated to traditional approaches. *Methods:* We propose a new multimodal approach that combines electrical sensing and optical imaging to classify pollen grains flowing in a microfluidic chip at a throughput of 150 grains per second. Electrical signals and synchronized optical images are processed by two independent machine learning-based classifiers, whose predictions are then combined to provide the final classification outcome. *Results:* The applicability of the method is demonstrated in a proof-of-concept classification experiment involving eight pollen classes from different taxa. The average balanced accuracy is 78.7 % for the electrical classifier, 76.7 % for the optical classifier and 84.2 % for the multimodal classifier. The accuracy is 82.8 % for the electrical classifier, 84.1 % for the optical classifier and 88.3 % for the multimodal classifier. *Conclusion:* The multimodal approach provides better classification results with respect to the analysis based on electrical or optical features alone. *Significance:* The proposed methodology paves the way for automated multimodal palynology. Moreover, it can be extended to other fields, such as diagnostics and cell therapy, where it could be used for label-free identification of cell populations in heterogeneous samples.**

***Index Terms*— Microfluidics, Impedance cytometry, Sensors, Machine learning, Automated palynology.**

I. Introduction

In this work, we present a novel multimodal analysis approach, based on electrical sensing and optical imaging, which is tailored to solve classification tasks in palynology.

Palynology is an interdisciplinary science that deals with the study of pollen and fungal spores and finds applications in many fields, including: ecology [1], aerobiology and air quality control [2], allergology and clinical immunology [3], as well as agriculture and food industry [4], economics [5], and criminology [6]. As an example, in agriculture, control over pollen quality and pollination along the pollen supply chain is a key success factor to ensure high quality seed and yield [7]. On the other hand, the main purpose of aerobiological monitoring is to know what types of biological particles are present and how their concentration in the atmosphere varies, influenced by meteorological and environmental factors that interact in the various stages of the reproductive process, release and transport. The World Allergy Organization (WAO) and the Global Alliance against Respiratory Diseases (GARD) indicate aerobiological monitoring as an important tool to improve the quality of life in an urban environment [8], [9], a goal defined among the urgency measures in several national laws (*e.g.* Italian Legislative Decree n. 111/2019).

The study of pollen and fungal spores takes place through microscopic analysis (optical or scansion electron microscope) of samples taken in the inspection site manually or using a sampling device (*e.g.*, impactor, cyclone, filter, spore trap) [10]. Typical particle sizes range between 1 and 100 µm, and the microscopic inspection usually involves labelling through a colorimetric or fluorescence stain to increase the contrast of the captured particles [10] (**Fig. S1** of the Supplementary Material). The identification and recognition of the different types of pollen and spores present in the samples is entrusted to specialized operators. The latter operate with the aid of photographic books, which contain images of the main plant taxa, and palinotheques prepared with fresh material of certain origin. This procedure requires long time and, despite being regulated by standardized methodologies governed by specific rules (*e.g.*, UNI EN 16868:2019 standard), it is subject to errors introduced in the different operational phases.

In the last two decades, there has been an increasing interest in the realization of automated procedures to speed up work and improve accuracy, through the development of principles and methods for automated palynology [11]. In fact, emerging new approaches to automatic pollen monitoring can, in principle, allow for real-time availability of the data with no human involvement [12]. On the other hand, systems for automated palynology may have drawbacks related to, *e.g.*, size of the instrumentation, high purchase and management costs of the equipment, and territorial scope of the application

This work was supported by the Mission Sustainability Programme of the University of Rome Tor Vergata under Grant E81I18000540005-SPY "Zero hunger with Superior Pollen and Yeast". (Corresponding author: Federica Caselli).

‡ M. D'Orazio and R. Reale contributed equally to this work.

F. Caselli is with the Department of Civil Engineering and Computer Science, University of Rome Tor Vergata 00133, Rome, Italy (e-mail: caselli@ing.uniroma2.it).

M. D'Orazio, A. Mencattini, and E. Martinelli are with the Department of Electronic Engineering, University of Rome Tor Vergata. R. Reale and P. Bisegna are with the Department of Civil Engineering and Computer Science, University of Rome Tor Vergata. A. De Ninno and L. Businaro are with the Institute for Photonics and Nanotechnology, Italian National Research Council. M. A. Brighetti and A. Travaglini are with the Department of Biology, University of Rome Tor Vergata.

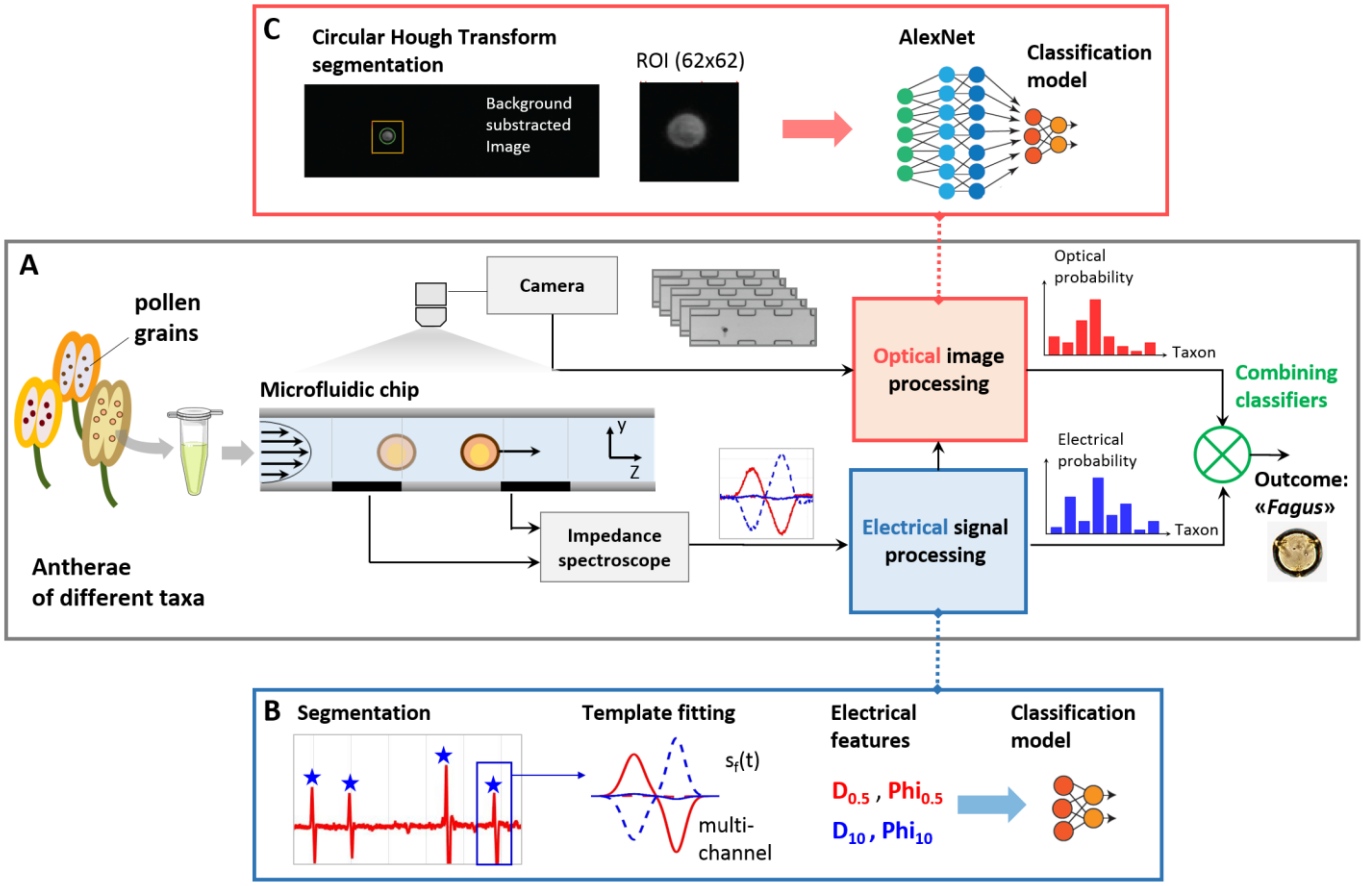

Fig. 1. System overview. (A) Schematic representation of the proposed multimodal analysis approach to taxon classification: electrical fingerprints and optical images of individual flowing grains from a mixture of taxa are simultaneously acquired and then independently processed, to obtain the electrical and optical probabilities of belonging to each taxon. The final classification outcome is obtained by combining the results of the two classifiers. (B) Electrical signal processing flow: segmentation, feature-extraction based on template-fitting, and classification. (C) Image-processing flow: background subtraction, ROI segmentation based on circular Hough transform, feature extraction by AlexNet, classification.

[13]–[15]. Notwithstanding the recent progress in automated palynology, the ideal system providing simplicity, portability as well as accuracy and consistency has yet to be developed [10], [11].

Currently, two types of technologies are most widely adopted for taxon-level automated classification of pollen [12], based on laser fluorescence or optical image recognition (or their combinations). Laser-induced fluorescence techniques to analyse atmospheric aerosols are commonly applied for research and human exposure monitoring [16]. However, measuring auto-fluorescence in itself may not provide sufficient specificity towards classification, and strong ultraviolet sources and high-performance optical components are required to detect weak autofluorescence signals, making the system relatively costly and bulky.

Recent works on automated palynology with optical images leverage on deep neural networks [14] and more precisely on convolutional neural networks (CNNs). CNNs consist in cascades of so-called convolutional layers, able to extract shift invariant features applying weight sharing across the two dimensions of the image, and max pooling layers which assure only maxima activations forward propagate. Neural network predictions are extremely fast, as the main computation consists in parallelizable matrix multiplications, which can be performed using optimized numeric libraries [17]. Daood et al. [18] adapted a pre-trained CNN network to a set of bright field and SEM images of pollen grains. This fine-tuning approach needs huge amount of data (10^5-10^6 samples) and a careful last layer re-training to prevent overfitting. As previously shown [19], the idea of using a pre-trained CNN for feature extraction and then exploiting the descriptors to train a standard machine learning classifier, demonstrated to be a very robust and efficient solution [20]. The selection of the layer for image coding and the feature selection strategy remain key factors deserving further investigation. In addition, the capability of the analysis platform to automatically locate the grains and encode them by CNN is also relevant, in particular in a high throughput analysis scenario.

Besides laser fluorescence and optical image recognition, the use of microfluidic impedance cytometry has recently been introduced as a novel tool for automated palynology [21], [22]. Microfluidic impedance cytometry is a non-invasive technique for the electrical characterization of single particles and cells at high throughput (a few hundreds of cells per second) [23]–[28]. Compared with traditional approaches for single-cell analysis like flow cytometry, its main advantages are the label-free nature, requiring minimal sample processing,

and the potential for low-cost and portable implementation [29]. The basic principle is as follows: (i) an AC electric field is established in a microchannel equipped with microelectrodes and filled with a conductive fluid; (ii) the field perturbation induced by the passage of a flowing particle is measured as an electric current signal; (iii) this signal depends on the intrinsic dielectric properties of the particle and therefore can be used for particle characterization. Biological cells are characterized by the presence of a lipid plasma membrane, exhibiting a capacitive behavior. Accordingly, at low frequencies (around 0.5 MHz in saline) the cell behaves like an insulating particle and the technique provides cell sizing. Impedance measurements in the 2-10 MHz frequency range give information on the cell membrane capacitance. Frequencies above 20 MHz probe internal properties of the cell [30]. Heidmann *et al.* [21] demonstrated that different stages of developing pollen, as well as dead, viable and germinating pollen populations could be detected and quantified by microfluidic impedance cytometry, using frequencies of 0.5 to 12 MHz. Canonge *et al.* [31] used the technique to track and characterize wheat microspores in androgenesis. However, the capabilities of impedance cytometry to discriminate among different pollen taxa has not yet been explored.

Optical imaging and impedance cytometry are quite different sensing modalities, and accordingly they probe particle properties of different nature. Therefore, a multimodal characterization based on both electrical and optical sensing modalities could improve the recognition accuracy with respect to the individual techniques. In order to test this hypothesis, herein we implement an original multimodal approach for label-free, high-throughput analysis of pollen grains based on electrical sensing and simultaneous optical imaging inside a microfluidic impedance cytometer. Moreover, we combine our microfluidic platform with a machine learning approach to data analysis, in order to increase robustness with respect to human-based analysis, and to speed up the analysis time, making data readily available.

An overview of the proposed system is provided in **Fig. 1**. Pollen grains from a mixture of taxa flow one-by-one through the microfluidic chip. The variation in channel impedance due to the passage of individual grains is recorded with an impedance spectroscope, while acquiring a high-speed optical video. Electrical signals and synchronized optical images are processed by two independent machine learning-based classifiers, providing the electrical and optical probability of belonging to the different taxa, respectively. These probabilities are then combined by applying a consensus paradigm to obtain the classification outcome [32]. Details of materials and methods are provided in Section 2, whereas the results of a proof-of-concept taxa classification experiment are reported in Section 3. Finally, conclusions are drawn.

II. Materials and Methods

A. Microfluidic Device

The device was fabricated with standard microfabrication techniques, as previously reported [33], [34]. Briefly, the chip consists of a glass microscope slide with integrated microelectrodes (Ti/Au, 20 nm/200 nm), bonded to a PDMS-embedded microchannel (**Fig. S2A-B** of the Supplementary Material). The PDMS microchannels were replica molded from photolitographically patterned SU-8 molds, while the electrodes were deposited on glass using optical lithography, e-beam evaporation and lift-off process. A simple design with four coplanar electrodes housed in lateral channels was used (**Fig. 2A-B**). Relevant dimensions are as follows: the main channel is 120 µm wide and 60 µm high; lateral channels are 90 µm wide and 90 µm apart from each other; the electrodes in the lateral channels have a 60 µm recess with respect to the main channel. Arrays of micro-pillars were included at the inlet fluidic port to reduce the risk of channel clogging (**Fig. S2C** of the Supplementary Material). A custom chip holder was used for fluidic and electric connections (**Fig. S2D** of the Supplementary Material).

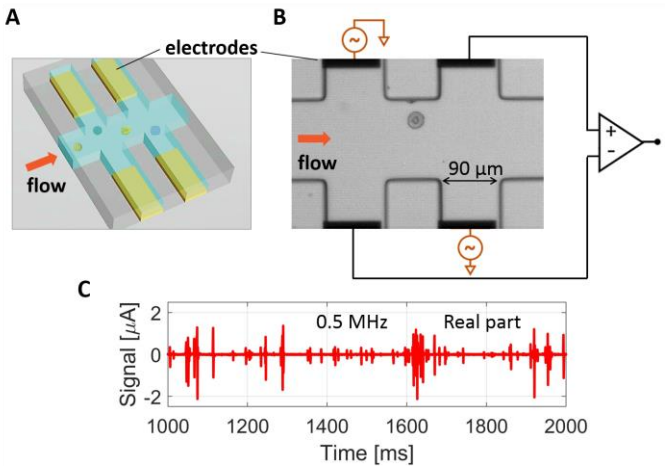

Fig. 2. (A) 3D schematic of the microfluidic impedance chip. (B) Microscopy image of the sensing region (top view) with illustration of the wiring scheme: a multifrequency AC signal is applied to diagonally opposite electrodes and the differential current from the other electrode pair is collected. (C) Portion of a typical data stream (real part of 0.5 MHz signal).

B. Sample Collection, Storage and Preparation

Pollen grains of six different taxa (*Cupressus*, *Fagus*, *Fraxinus*, *Juglans*, *Ligustrum*, *Ostrya*) were collected in Lazio (Italy) by the Aerobiological Monitoring Center of the University of Rome Tor Vergata. The harvest of pollen for storage was done by collecting entire inflorescences or male flowers or single anthers according to the characteristics of the flower. Anthers or flowers were carried in laboratory where pollen was collected by using tweezers and scissors and placed in small plastic baggies or Eppendorf tubes. The specimen were identified using different plants Key [35], [36]. For upgrading nomenclature the Angiosperm Phylogeny Website was consulted [37]. Eppendorf tubes were stored in closed cabinet with silica gel.

Before the experiments, pollen grains were suspended in a saline buffer. The buffer was augmented with 150 mg/ml

sucrose, to reduce grain sedimentation, and spiked with 10 μm diameter polystyrene beads (Sigma-Aldrich), as internal reference for the impedance measurements. Final sample concentrations were in the order of 10^5 grains/ml for each taxon, and 10^4 beads/ml for the beads. Samples were filtered with 50 μm filters (Cell Tricks) to prevent the risk of channel clogging. Samples were injected into the microfluidic chip by a syringe pump (Harvard Apparatus) at a rate of 90 μl/min.

When suspended in a liquid buffer, *Cupressus* grains undergo a hydration that may cause the splitting of the exine (the outer layer of the pollen grain wall) and a huge swelling of the intine [38], [39] (the innermost layer of the pollen grain wall). Accordingly, *Cupressus* grains can be found in the suspension in three different statuses: intact *Cupressus* grain, *Cupressus* grain without exine, split-off exine shell (cf. also **Fig. 3F-H** and **Fig. S5** of the Supplementary Material). A total of eight classes (besides the reference beads) is therefore considered in the classification problem.

C. Impedance Acquisition and Analysis

Electrical measurements were performed using an impedance spectroscope (HF2IS, Zurich Instruments, sampling rate 210 Msample per second), along with a transimpedance amplifier (HF2TA, Zurich Instruments) for signal conditioning. As shown in **Fig. 2B,** AC voltage was applied to diagonally opposite electrodes and the differential current flowing through the other electrodes was demodulated and recorded (demodulator readout rate 115 ksample per second, 20 kHz filter bandwidth). In order to characterize the grain dielectric behaviour, the measurements were carried out at two simultaneous frequencies (0.5 and 10 MHz, 5 V each). Two signals (real and imaginary components) were recorded from each frequency channel. Accordingly, each grain is characterized by an electrical fingerprint composed of four signals. A portion of an exemplary data steam is shown in **Fig. 2C**.

The selected wiring scheme was introduced by our group [33] to mitigate the measurement blurring induced by different particle trajectories [40], without the need for particle focusing systems. In fact, upon the passage of a flowing particle (herein, a pollen grain) the recorded current exhibits two subsequent pulses with opposite sign and generally different amplitude. The relative difference of positive and negative pulse amplitudes is an electrical metric that correlate with particle trajectory and therefore can be exploited to remove positional dependence from the measured signals via simple calibration, with a sensible increase in accuracy [33]. Upon calibration, the cube root of pulse amplitude average (i.e., the electrical diameter) and its phase are computed [41]. Electrical diameter and phase are widely adopted in microfluidic impedance cytometry as metrics for cell phenotyping and classification [30].

The main steps of the electrical signal processing flow are shown in **Fig. 1B**. The recorded impedance data stream was segmented to identify grain passage in the sensing region. The measured throughput was around 150 particles/s. A multi-frequency complex bipolar Gaussian template was fitted to each detected event and the optimal fitting parameters were used to compute the electric diameter (D) and phase (Phi) at 0.5 and 10 MHz (cf. **Fig. S3** of the Supplementary Material for details). The four electrical features ($D_{0.5}$, D_{10}, $Phi_{0.5}$, Phi_{10}) were used to build a support vector machine (SVM) classification model [42], with the Linear kernel and a One-Versus-One approach for multiclass prediction. The dataset was pre-scaled before its use in the training and validation procedures [43]. The Matlab SVM implementation with default settings was used for data analysis. The model returns the (electrical) sample-probability of belonging to each class. The dataset was randomly split in training set and test set in equal proportions (for each class). This procedure was repeated 100 times to ensure statistical significance and avoid bias due to random subsampling.

D. Image Acquisition and Analysis

The sample flow through the detection area was acquired using a high-speed camera (Photron Mini UX100, frame rate 4000 fps, shutter time 3.9 μs) connected to an inverted microscope (Zeiss Axio Observer, 10x objective). With the present frame rate, field of view and particle throughput, only 20 % of the recorded frames displayed flowing particles. The optical image acquisition was synchronized with the impedance measurements. Accordingly, the image frames containing pollen grains could be straightforwardly identified based on the segmentation of the impedance data stream, with considerable saving of computational time. In particular, for each event detected in the electrical data stream, five synchronized frames in the temporal neighbourhood of the electrical trigger were processed, in favour of robustness of the image analysis.

The image-processing flow is as follows (**Fig. 1C**). First, background suppression procedure and scaling to [0, 1] were applied to each image frame. Automatic pollen localization was performed through Circular Hough Transform (CHT) [44], a method specifically designed to detect circles in a given image. The radius range for the searching was set to [15, 25] px (*i.e.*, [14.15, 23.58] μm). A 62 x 62 px Region Of Interest (ROI) was then extracted around each detected circle. The ROI dimension was selected according to the average dimension of pollen grains. Using a bilinear interpolation method the ROI was then reshaped to 227 x 227 px in order to match the input size of the AlexNet deep pre-trained CNN [45], [46]. This network was trained over 1.2 million high-resolution images from the ImageNet database to classify objects in 1000 categories. To exploit AlexNet's representation power, we extracted artificial neuron's activations out of the 3th Max Pooling Layer (pool5) of the network, using a transfer learning approach and avoiding retraining.

The same 100 repartitions of the dataset in training set and test set as used for the electrical analysis were considered. A stepwise feature selection procedure [47] was applied to each training set. In particular, we used MATLAB® 2020b

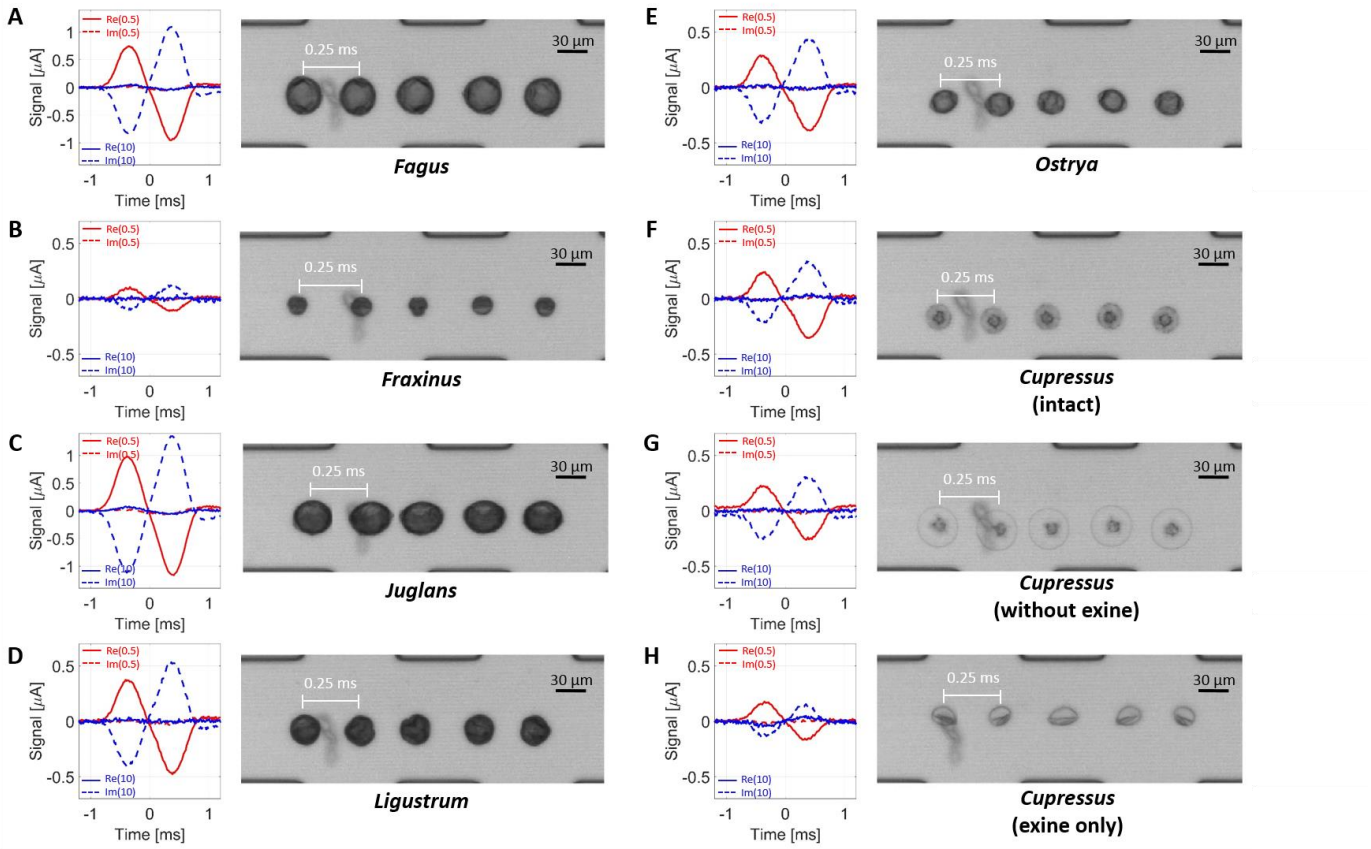

Fig. 3. Representative electrical signals (continuous line, real part; dotted line, imaginary part; red, 0.5 MHz; blue 10 MHz) and synchronized optical images (overlay of five frames, 0.25 ms time lapse). One example of each taxa is shown: (A) *Fagus*, (B) *Fraxinus*, (C) *Juglans*, (D) *Ligustrum*, (E) *Ostrya*, (F) intact *Cupressus* grain, (G) *Cupressus* without exine, (H) exine of *Cupressus* grain. An imperfection of the microchannel is found in the optical images, probably due to debris material sticking on the channel floor. That artefact did not affect the image processing procedure, thanks to background subtraction.

stepwisefit (with parameter 'penter' set to 0.05). The selected set of features was then used to build the classification model and evaluate performances on the test set. In this way, we tackle the need for thousands of data while improving the statistical significance of the obtained results. The selected training features (27 ± 3 in number, depending on the training set) were then autoscaled and used to build an SVM classification model [42] with a linear kernel function and the same settings used with the impedance features. The model returns the (optical) sample-probability of belonging to each class. Since for each grain detected in the impedance data stream five image frames are processed, we considered the average posterior probability to belong to each class over the five frames. The sample was assigned to the class with the highest average probability.

E. Combining Classifiers

In the present multimodal framework, electrical signals and optical images are acquired. While it could be possible to use a single SVM classifier based on the whole set of electrical and optical features, two SVM classifiers are used in this work, to preserve the physically different information of the impedance data with respect to the optical ones. Accordingly, each classifier (electrical or optical) uses its own representation of the input (the pollen grain). A common theoretical framework for classifier combination in such kind of scenario was developed by Kittler *et al.* [32], who derived as special cases the commonly used classifier combination schemes such as product rule, sum rule, min rule, max rule, median rule, and majority voting. In the present work, those combination schemes were initially implemented and compared (results not shown). The product rule outperformed other classifier combinations schemes and was selected for the analysis.

F. Expert Human Classifier

In order to establish the performance of the electrical, optical and multimodal classifiers a ground truth is needed. To this aim, the grains were labelled by an expert human. In particular, the expert was asked to indicate the taxon of each grain on the basis of the five frames recorded as the grain was flowing in the sensing region of the microfluidic chip (**Fig. S4** of the Supplementary Material).

III. Results and Discussion

As shown in **Fig. S1** of the Supplementary Material, during traditional microscopic analysis fuchsin staining is usually exploited for the identification of pollen grains compared to

Fig. 4. The figure reports the electrical features of nine grains for each class (row by row). For each grain, the four electrical features are visualized with a bar plot. Feature ordering in each bar plot is (from left to right): electrical diameter at 0.5 MHz (red), phase shift at 0.5 MHz (orange), electrical diameter at 10 MHz (blue), and phase shift at 10 MHz (cyan). The features were normalized by subtracting the median value and dividing by the interquartile range. Grain samples framed in green were correctly classified by the electrical method, whereas samples framed in red were wrongly classified.

any other body in the image, such as for example air bubbles, dust or debris. In fact, the cell wall of the pollen grain is rich in sporopollenin, a protein that turns red-fuchsia if it comes into contact with a solution containing fuchsin, and therefore this coloring can be used as a discriminating characteristic. The ability to deal with lots of debris has been indicated as a requirement for automation in palynology [11]. In the proposed label-free multimodal approach, small dust and debris are distinguishable from pollen grains on the basis of their lower electric diameter (cf. also **Fig. S5** of the Supplementary Material), while possible air bubbles, which are non-conductive, generate high-amplitude signal spikes that are easily discarded from the data stream by thresholding. In fact, an initial selection of the events to be processed by the optical classifier is performed on the basis of the impedance analysis, thus further reducing the burden of image processing. On the other hand, optical images can validate the relationship between electrical signatures and particle geometry or position [48], [49].

A representative gallery of the acquired signals/images is shown in **Fig. 3**. One example for each of the eight classes is considered. In particular, the measured electrical signals are reported (real and imaginary parts, at 0.5 and 10 MHz) along with an overlay of the five matched optical frames. Overall, more than six hundred electrical fingerprints and three thousand optical images were acquired.

Regarding the electrical signals, in all cases the real part of the low-frequency current and the imaginary part of the high-frequency current are dominant with respect to the other two signals (namely, imaginary part at low frequency and real part at high frequency). The relative difference of positive and negative peak amplitudes is small, in agreement with the fact that they refer to centered or slightly off-centered grains (as shown by the images). An important variation of signal amplitude among the different taxa is noticed, with *Fraxinus* (B) and *Cupressus* exine (H) providing the smallest signals (around 0.1-0.2 μA) and *Fagus* (A) and *Juglans* (C) providing the highest signals (around 1 μA).

By examining the optical images, noticeable differences between the various taxa are found, in terms of grain size, morphology, grey-level intensity, and texture. Interestingly, while in general there is a correlation between the grain size

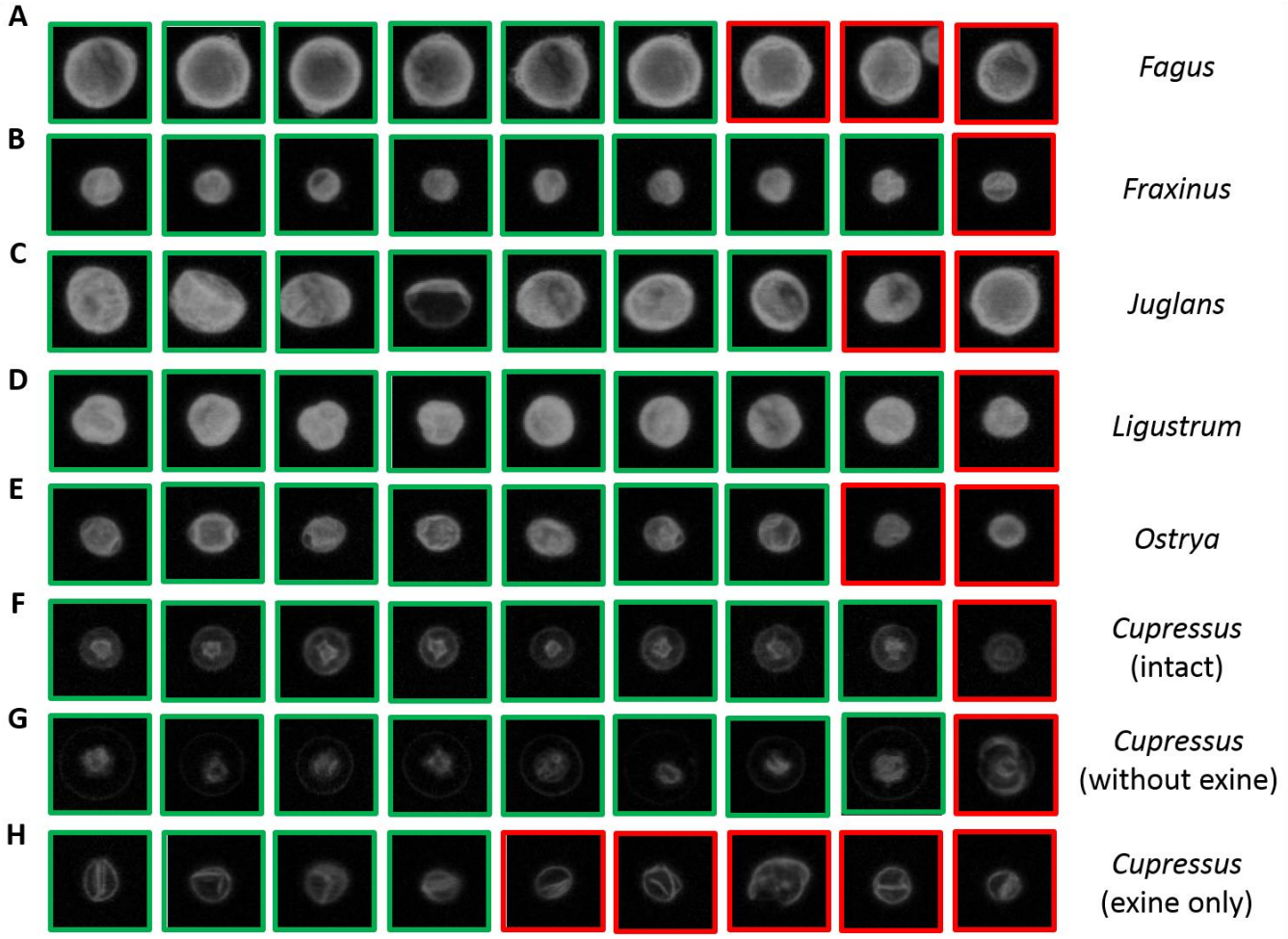

Fig. 5. The figure reports nine ROI samples for each class (row by row). Samples mounted in green were correctly classified by the optical method, whereas samples framed in red were wrongly classified.

(as revealed in the image frame) and the electrical signal amplitude, this is not the case for the *Cupressus* without exine (G). The latter is characterized by an expanded intine (which is hydrated and no longer compressed by the exine shell) and has a size comparable to that of *Fagus* (A) and *Juglans* (C) grains (*i.e.*, about 30 μm diameter). However, its electrical signals are significantly smaller (around 0.25 μA vs. 1 μA). This suggests that the hydrated intine offers a lower hindrance to the electric current flow with respect to the exine material. The dynamics of the hydration process of *Cupressus* grains, as monitored by impedance measurements, is reported in **Fig. S6** of the Supplementary Material.

The performances of the individual classifiers (electrical or optical) were first investigated. **Figure 4** shows representative outcomes of the electrical classifier. In particular, nine grain samples for each class are reported, based on the classification made by the human expert. For each grain, a bar plot showing the four electrical features is shown. Samples mounted in green were correctly classified by the electrical method, whereas samples framed in red were wrongly classified (cf. also **Fig. S7** and **Fig. S8** of the Supplementary Material). **Figure 5** shows representative outcomes of the optical classifier. Nine randomly chosen ROIs for each taxon are considered. As in **Figure 4**, they are framed in green [resp. red] in case of right [resp. wrong] classification. The images show the heterogeneity inside each class. A coincidence (*i.e.*, two grains traveling through the microchannel in close proximity) is found in panel (A), second-last.

Representative confusion matrices obtained by testing the optical and electrical classifiers on one of the test sets (randomly chosen among the 100 repartitions) are shown in **Fig. 6A** and **B**, respectively. As shown by the confusion matrices, even though during sample preparation approximately the same concentration for each taxon was pursued, the fraction of grains that reach the electrical sensing zone is not the same for all taxa, resulting in imbalanced class distribution. In particular, *Fagus* is the least represented class. This can be explained on the basis of the size of the grain (around 35 μm) and its sticky nature, which may compromise the passage of *Fagus* grains through the filters and the anti-clogging pillars in the microchannel.

With the electrical classifier, five classes (*Fraxinus*, *Juglans*, *Ligustrum*, intact *Cupressus*, *Cupressus* exine) were classified with a recall (*i.e.*, number of correctly classified grains over total number of grains of the class) higher than 84 %. A lower recall was obtained for *Fagus* (77.8 %), *Cupressus*

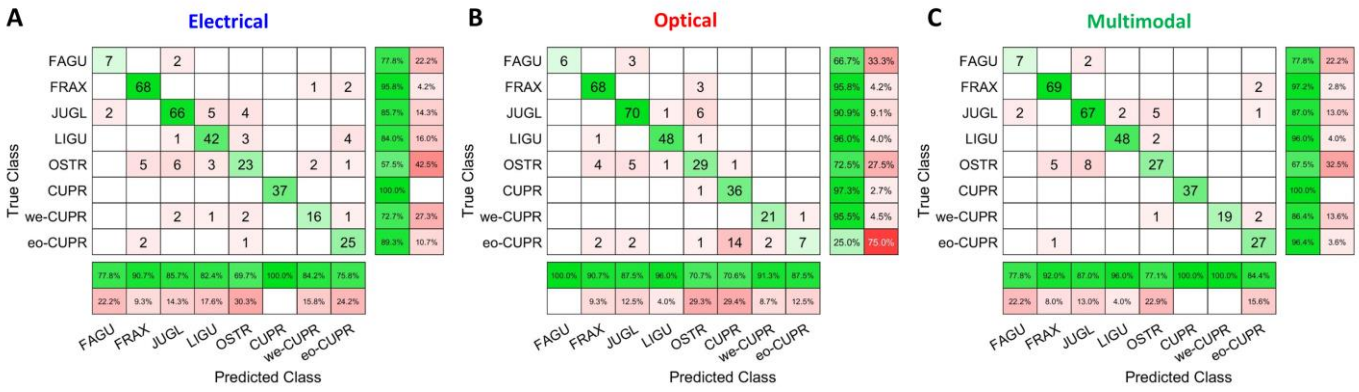

Fig. 6. Representative confusion matrices obtained with the (A) electrical, (B) optical, and (C) multimodal classifiers. Normalizations by row (i.e., recall) and by column (i.e., precision) are also reported. Class labels are as follows: FAGU, *Fagus*; FRAX, *Fraxinus*; JUGL, *Juglans*; LIGU, *Ligustrum*; OSTR, *Ostrya*; CUPR, intact *Cupressus*; we-CUPR, *Cupressus* without exine; eo-CUPR, *Cupressus* exine.

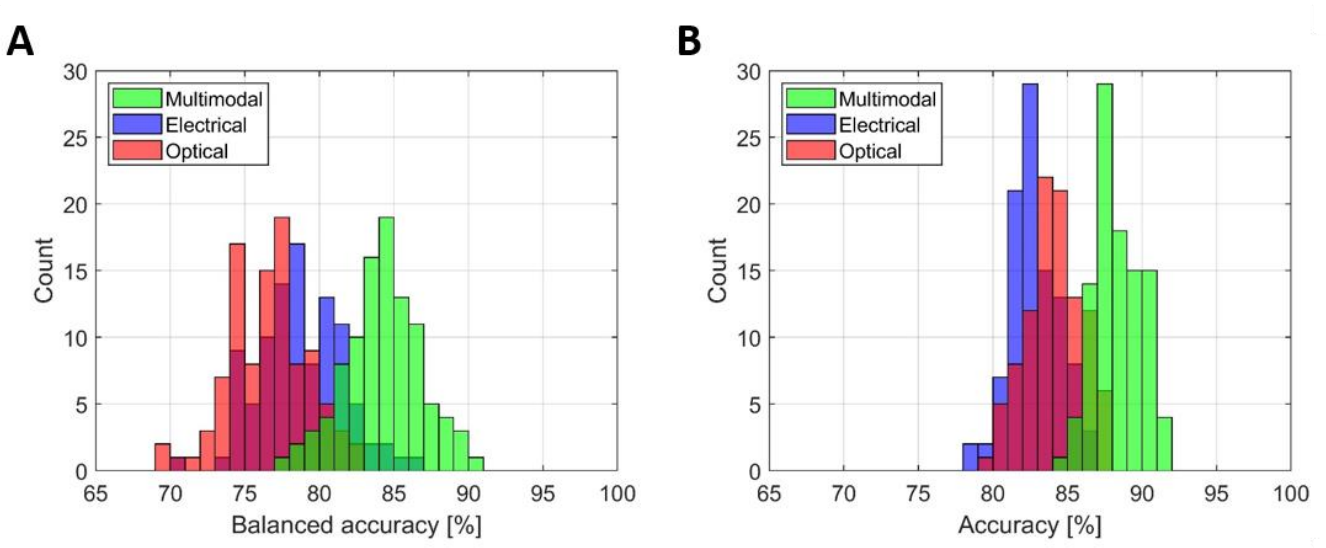

Fig. 7. Histograms of (A) balanced accuracy and (B) accuracy, relevant to the 100 different partitions of the dataset. The performances of the electrical, optical and multimodal classifiers are shown in blue, red, and green, respectively.

without exine (72.7 %), and *Ostrya* (57.5 %). With the optical classifier, five taxa (*Fraxinus*, *Juglans*, *Ligustrum*, intact *Cupressus*, *Cupressus* without exine) were classified with a recall higher than 90 %. A lower recall was obtained for *Ostrya* (72.5 %), *Fagus* (66.7 %), and *Cupressus* exine (25 %). The lowest precision (*i.e.*, number of correctly classified grains over total number of grains attributed to the class) was around 70% for both classifiers, and was associated to *Ostrya* (electrical classifier) and *Ostrya* or intact *Cupressus* (optical classifier).

The performance of the multimodal classifier was then investigated and compared with those of the electrical and optical classifiers. **Figure 6C** shows the confusion matrix obtained with the multimodal classifier for the same test set considered in panels **A** and **B**. For five taxa, the recall of the multimodal approach is greater than or equal to the best between the two single approaches. For none of the other taxa, it is lower than the worst of both single approaches. Analogous results hold for the precision. The multimodal approach significantly improves the unsatisfactory recalls of each single classifier (i.e., *Ostrya* for the electrical classifier, and *Cupressus* exine for the optical classifier). Moreover, the minimum recall over the eight classes is 67.5 % (*Ostrya*), which is significantly higher than that obtained with the electrical or optical classifier (57.5 % and 25%, respectively). The minimum precision is 77.1 % (*Ostrya*), which compares favourably with that of the individual classifiers (around 70%). Overall, the multimodal classifier preserves the good performances obtained with one or another single approach, resulting in a substantial improvement compared to the more unsatisfactory results of a single classifier. In other words, both single methods can be successfully used for a subset of pollen classes, whereas the multimodal classifier works nicely with the whole ensemble (for both recall and precision).

The performance of the three classifiers (electrical, optical, and multimodal) over all the 100 repartitions of the dataset are reported in **Fig. 7**. In particular, the histograms of the balanced accuracy (*i.e.*, the average of the recall obtained on each class) and of the accuracy (overall recall) are shown in **Fig. 7A** and **B**, respectively. The balanced accuracy is insensitive to

imbalanced class distribution and it gives more weight to the instances coming from minority classes. On the other hand, the accuracy treats all instances alike and usually favors the majority class. According to both metrics, the multimodal classifier outperforms the single classifiers. In particular, the average balanced accuracy is 78.7 % for the electrical classifier, 76.7 % for the optical classifier and 84.2 % for the multimodal classifier. The accuracy is 82.8 % for the electrical classifier, 84.1 % for the optical classifier and 88.3 % for the multimodal classifier.

These results show that a multimodal characterization is able to increase the classification accuracy with respect to an analysis based on electrical or optical features alone. In fact, the combination of electrical and optical properties serves as a valuable set of complementary intrinsic markers for single-grain analysis, providing better differentiation of pollen taxa.

The performance of each classifier (electrical or optical), and therefore the performance of the multimodal classifier, could be further improved. In particular, impedance spectroscopy at eight (rather than two) simultaneous frequencies [50] could enrich the impedance-based characterization. In case of biological cells, the measured impedance spectra are usually fitted with single- or multi-shell dielectric models [50], [51], to provide values of dielectric parameters of subcellular structures (*e.g.*, membrane capacitance, cytoplasm conductivity and permittivity). In Sukhorukov *et al.* [52], a single-shell model was used to fit electrorotation spectra of pollen grains of *Lilium longiflorum.* However, a comprehensive analysis of the dielectric structure (and corresponding models) of pollen grains of the various taxa has yet to be performed.

Machine learning approaches have been used in combination with microfluidic impedance cytometry to classify biological cells based on electrical features. Ahuja *et al.* [53] used an SVM classifier to discriminate between live and dead T47D breast cancer cells. Yang *et al.* [54] used a backpropagation neural network to classify MCF-7 breast cancer cells in a 3-class classification problem. To the best of the Authors' knowledge, this is the first time that electrical features are successfully used in an 8-class classification task. On the other hand, image-based approaches to classification tasks involving 8 classes or more were reported in the literature. Sevillano et al. [55] reported proper classification of pollen grains from a dataset with up to 46 different classes, produced by the Classifynder classification system. The acquisition throughput was lower than 0.2 grains per second. Microfluidic approaches such as the one proposed in this work may enable higher throughput (150 grains per second in our case). Kleiber *et al.* [56] recently demonstrated a microfluidic system wherein each pollen grain is visualized under different angles of view by purposely inducing rotation with 3-step flow focusing. The system was applied for population analysis of 15 pollen species using deep convolutional neural networks at up to 56 grains per second. That multidirectional imaging approach enables a more exhaustive optical representation with respect to the 2D imaging modality and could be integrated within our multimodal approach, to confer increased robustness to the optical features. In addition, an increase of the number of collected samples (*e.g.,* 1000 per class) would improve the training performance of the deep learning architecture to reach higher accuracy.

Higher acquisition throughputs could be achieved by implementing strategies for coincidence arbitration [57]. Higher processing throughputs, which are needed in case of online processing, could be obtained by using neural networks to process the impedance data stream [58], besides the optical images. Moreover, the introduction of constriction structures or deformation regions in the channel could provide information on pollen mechanical properties [54], [59], a topic which is gaining increasing attention [60], [61].

In the present multimodal strategy, two independent (electrical and optical) SVM classifiers were used. It could be interesting to investigate the possibility to implement a weighted adaptive combination of classifiers [62], [63]. According to the definition of a sort of real-time reliability level of each modality, the different probability could be combined using for example a weighted product rule in which the weight is tuned according to the ongoing reliability level. Such improved strategy may help deal with occasional faults or decision failures. Finally, in order to achieve full automation in pollen analysis, the next step is the integration of the proposed microfluidic system with an automatic sampling method (*e.g.*, for airborne pollen), to enable the acquisition of data at predetermined time intervals, human workload reduction and rapid online pollen reporting.

IV. Conclusions

We have proposed a multimodal approach for high-throughput automated palynology based on microfluidic impedance cytometry and simultaneous optical imaging. Electrical fingerprints and optical images both provide high-content information useful for pollen analysis and taxa classification. Their use in combination outperforms the individual approaches. Moreover, impedance analysis enables to discard dust and small debris based on their electrical diameter, and using the impedance signals as pointers to image frames significantly reduces the cost of image processing. Future applications could address, *e.g.*, the classification of pollen grains based on the presence of pollutants, to shed light into the relationships among atmospheric pollutants, pollen grains and their allergenicity, which are still not completely understood [64], [65]. The system is adaptable to the needs of the different research fields dealing with classification of biological particles with dimensions between 10 and 100 μm. The multimodal approach introduced in this work for pollen classification can be of interest for the broad community of biophysical cytometry [66], for applications dealing with label-free single-cell phenotyping. The combination of microfluidics, machine learning, and multimodal analysis can serve as a stepping stone for the development of next generation systems for single-cell analysis.

REFERENCES

[1] A. M. Mercuri, M. Marignani, and L. Sadori, "2013 Palynology: The bridge between palaeoecology and ecology for the understanding of human-induced global changes in the Mediterranean Area," *Ann. Bot. - Italy*, vol. 3, pp. 107–113, 2013, doi: 10.4462/annbotrm-10332.

[2] A. Di Menno di Bucchianico *et al.*, "Combined effects of air pollution and allergens in the city of Rome," *Urban For. Urban Green.*, vol. 37, pp. 13–23, 2019, doi: 10.1016/j.ufug.2018.04.001.

[3] M. Di Fraia *et al.*, "Adherence to prescribed e-diary recording by patients with seasonal allergic rhinitis: Observational study," *J. Med. Internet Res.*, vol. 22, no. 3, p. e16642, Mar. 2020, doi: 10.2196/16642.

[4] S. Padureanu and A. Patras, "Palynological characterization, germination potential and pollen tube growth of direct producer hybrids Noah and Othello (Vitis genus)," *Flora: Morphol. Distrib. Funct. Ecol. Plants*, vol. 240, pp. 58–67, 2018, doi: 10.1016/j.flora.2018.01.005.

[5] A. Izdebski, G. Koloch, T. Słoczyński, and M. Tycner, "On the use of palynological data in economic history: New methods and an application to agricultural output in Central Europe, 0-2000AD," *Explor. Econ. Hist.*, vol. 59, pp. 17–39, 2016, doi: 10.1016/j.eeh.2015.10.003.

[6] S. S. Alotaibi *et al.*, "Pollen molecular biology: Applications in the forensic palynology and future prospects: A review," *Saudi Journal of Biological Sciences*, vol. 27, no. 5. pp. 1185–1190, 2020, doi: 10.1016/j.sjbs.2020.02.019.

[7] "Ampasys A.G." https://amphasys.com/.

[8] G. D'Amato *et al.*, "Meteorological conditions, climate change, new emerging factors, and asthma and related allergic disorders. A statement of the World Allergy Organization," *World Allergy Organization Journal*, vol. 8, no. 1. pp. 1–52, 2015, doi: 10.1186/s40413-015-0073-0.

[9] Global Alliance of Chronic Respiratory Diseases, "COVID-19 pandemic alert: time to focus on lung health-Beijing call to action for lung health promotion," *J. Thorac. Dis.*, vol. 12, no. 6, pp. 3238–3241, 2020, doi: 10.21037/jtd-gard-20-002.

[10] Y. Wu *et al.*, "Label-Free Bioaerosol Sensing Using Mobile Microscopy and Deep Learning," *ACS Photonics*, vol. 5, no. 11, pp. 4617–4627, 2018, doi: 10.1021/acsphotonics.8b01109.

[11] K. A. Holt and K. D. Bennett, "Principles and methods for automated palynology," *New Phytol.*, vol. 203, no. 3, pp. 735–742, 2014, doi: 10.1111/nph.12848.

[12] I. Šauliene *et al.*, "Automatic pollen recognition with the Rapid-E particle counter: The first-level procedure, experience and next steps," *Atmos. Meas. Tech.*, vol. 12, no. 6, pp. 3435–3452, 2019, doi: 10.5194/amt-12-3435-2019.

[13] C. Chappuis, F. Tummon, B. Clot, T. Konzelmann, B. Calpini, and B. Crouzy, "Automatic pollen monitoring: first insights from hourly data," *Aerobiologia (Bologna).*, vol. 36, no. 2, pp. 159–170, 2020, doi: 10.1007/s10453-019-09619-6.

[14] J. Schiele *et al.*, "Automated Classification of Airborne Pollen using Neural Networks," in *Proceedings of the Annual International Conference of the IEEE Engineering in Medicine and Biology Society, EMBS*, 2019, pp. 4474–4478, doi: 10.1109/EMBC.2019.8856910.

[15] A. Travaglini, M. A. Brighetti, G. Bianchi, E. Taschini, S. Estivi, and G. Piovesan, "Pollentrack: automated reading OM (optical microscope) of pollen and spores," in *Abstract Book of the Mediterranean Palynology Symposium*, 2015, p. 117.

[16] B. E. Swanson and J. A. Huffman, "Development and characterization of an inexpensive single-particle fluorescence spectrometer for bioaerosol monitoring," *Opt. Express*, vol. 26, no. 3, p. 3646, 2018, doi: 10.1364/oe.26.003646.

[17] P. Eulenberg *et al.*, "Reconstructing cell cycle and disease progression using deep learning," *Nat. Commun.*, vol. 8, no. 1, pp. 1–6, 2017, doi: 10.1038/s41467-017-00623-3.

[18] A. Daood, E. Ribeiro, and M. Bush, "Pollen grain recognition using deep learning," in *Lecture Notes in Computer Science (including subseries Lecture Notes in Artificial Intelligence and Lecture Notes in Bioinformatics)*, 2016, vol. 10072 LNCS, pp. 321–330, doi: 10.1007/978-3-319-50835-1_30.

[19] V. Sevillano and J. L. Aznarte, "Improving classification of pollen grain images of the POLEN23E dataset through three different applications of deep learning convolutional neural networks," *PLoS One*, vol. 13, no. 9, p. e0201807, 2018, doi: 10.1371/journal.pone.0201807.

[20] J. Yosinski, J. Clune, Y. Bengio, and H. Lipson, "How transferable are features in deep neural networks?," in *Advances in Neural Information Processing Systems*, 2014, vol. 4, no. January, pp. 3320–3328.

[21] I. Heidmann, G. Schade-Kampmann, J. Lambalk, M. Ottiger, and M. Di Berardino, "Impedance Flow Cytometry: A Novel Technique in Pollen Analysis," *PLoS One*, vol. 11, no. 11, pp. 1–15, 2016, doi: 10.1371/journal.pone.0165531.

[22] L. Ascari *et al.*, "Hazelnut Pollen Phenotyping Using Label-Free Impedance Flow Cytometry," *Front. Plant Sci.*, vol. 11, p. 615922, 2020, doi: 10.3389/fpls.2020.615922.

[23] E. Rollo *et al.*, "Label-free identification of activated T-lymphocytes through tridimensional microsensors on chip," *Biosens. Bioelectron.*, vol. 94, pp. 193–199, 2017, doi: 10.1016/j.bios.2017.02.047.

[24] I. Bilican, M. T. Guler, M. Serhatlioglu, T. Kirindi, and C. Elbuken, "Focusing-free impedimetric differentiation of red blood cells and leukemia cells: A system optimization," *Sens. Actuator B-Chem.*, vol. 307, p. 127531, 2020, doi: 10.1016/j.snb.2019.127531.

[25] F. Caselli and P. Bisegna, "A simple and robust event-detection algorithm for single-cell impedance cytometry," *IEEE Trans Biomed Eng*, vol. 63, no. 2,

pp. 415–422, 2016, doi: 10.1109/TBME.2015.2462292.

[26] Z. Zhu *et al.*, "Using microfluidic impedance cytometry to measure C. elegans worms and identify their developmental stages," *Sens. Actuator B-Chem.*, vol. 275, pp. 470–482, 2018, doi: 10.1016/j.snb.2018.07.169.

[27] V. Farmehini *et al.*, "On-chip impedance for quantifying parasitic voltages during ac electrokinetic trapping," *IEEE Trans. Biomed. Eng.*, vol. 67, no. 6, pp. 1664–1671, 2020, doi: 10.1109/TBME.2019.2942572.

[28] L. Do Quang *et al.*, "Biological Living Cell in-Flow Detection Based on Microfluidic Chip and Compact Signal Processing Circuit," *IEEE Trans. Biomed. Circuits Syst.*, vol. 14, no. 6, pp. 1371–1380, 2020, doi: 10.1109/TBCAS.2020.3030017.

[29] C. Petchakup, K. H. H. Li, and H. W. Hou, "Advances in single cell impedance cytometry for biomedical applications," *Micromachines*, vol. 8, no. 3, p. 87, 2017, doi: 10.3390/mi8030087.

[30] C. Honrado, P. Bisegna, N. S. Swami, and F. Caselli, "Single-cell microfluidic impedance cytometry: from raw signals to cell phenotypes using data analytics," *Lab Chip*, vol. 21, no. 1, pp. 22–54, 2021, doi: 10.1039/D0LC00840K.

[31] J. Canonge, M. Philippot, C. Leblanc, P. Potin, and M. Bodin, "Impedance flow cytometry allows the early prediction of embryo yields in wheat (Triticum aestivum L.) microspore cultures," *Plant Sci.*, vol. 300, p. 110586, 2020, doi: 10.1016/j.plantsci.2020.110586.

[32] J. Kittler, M. Hatef, R. P. W. Duin, and J. Matas, "On combining classifiers," *IEEE Trans. Pattern Anal. Mach. Intell.*, vol. 20, no. 3, pp. 226–239, 1998, doi: 10.1109/34.667881.

[33] F. Caselli, A. De Ninno, R. Reale, L. Businaro, and P. Bisegna, "A novel wiring scheme for standard chips enabling high-accuracy impedance cytometry," *Sens. Actuator B-Chem.*, vol. 256, pp. 580–589, 2018, doi: 10.1016/j.snb.2017.10.113.

[34] R. Reale, A. De Ninno, L. Businaro, P. Bisegna, and F. Caselli, "Electrical measurement of cross-sectional position of particles flowing through a microchannel," *Microfluid. Nanofluidics*, vol. 22, no. 4, pp. 1–13, 2018, doi: 10.1007/s10404-018-2055-3.

[35] S. Pignatti, *Flora d'Italia*, 1st ed. Edagricole, Bologna, 1982.

[36] S. Pignatti, R. Guarino, and M. La Rosa, *Flora d'Italia*, 2nd ed. Edagricole-New Business Media, Bologna, 2017.

[37] P. F. Stevens, "Angiosperm Phylogeny Website," 2001. http://www.mobot.org/MOBOT/research/APweb/.

[38] M. Nepi, M. Guarnieri, S. Mugnaini, L. Cresti, E. Pacini, and B. Piotto, "A modified FCR test to evaluate pollen viability in Juniperus communis L.," *Grana*, vol. 44, no. 3, pp. 148–151, 2005, doi: 10.1080/00173130510010576.

[39] E. Duhoux, "Mechanism of exine rupture in hydrated taxoid type of pollen," *Grana*, vol. 21, no. 1, pp. 1–7, 1982, doi: 10.1080/00173138209427673.

[40] H. Daguerre, M. Solsona, J. Cottet, M. Gauthier, P. Renaud, and A. Bolopion, "Positional dependence of particles and cells in microfluidic electrical impedance flow cytometry: origin, challenges and opportunities," *Lab Chip*, vol. 20, no. 20, pp. 3665–3689, 2020, doi: 10.1039/d0lc00616e.

[41] A. De Ninno *et al.*, "High-throughput label-free characterization of viable, necrotic and apoptotic human lymphoma cells in a coplanar-electrode microfluidic impedance chip," *Biosens. Bioelectron.*, vol. 150, p. 111887, 2020, doi: 10.1016/j.bios.2019.111887.

[42] C. Cortes and V. Vapnik, "Support-vector networks," *Mach. Learn.*, vol. 20, no. 3, pp. 273–297, 1995, doi: 10.1007/bf00994018.

[43] V. Kecman, T.-M. Huang, and M. Vogt, "Iterative Single Data Algorithm for Training Kernel Machines from Huge Data Sets: Theory and Performance," in *Support Vector Machines: Theory and Applications*, 2005, pp. 255–274.

[44] T. J. Atherton and D. J. Kerbyson, "Size invariant circle detection," *Image Vis. Comput.*, vol. 17, no. 11, pp. 795–803, 1999, doi: 10.1016/s0262-8856(98)00160-7.

[45] A. Krizhevsky, I. Sutskever, and G. E. Hinton, "ImageNet classification with deep convolutional neural networks," *Commun. ACM*, vol. 60, no. 6, pp. 84–90, 2017, doi: 10.1145/3065386.

[46] A. Mencattini *et al.*, "Discovering the hidden messages within cell trajectories using a deep learning approach for in vitro evaluation of cancer drug treatments," *Sci. Rep.*, vol. 10, no. 1, pp. 1–11, 2020, doi: 10.1038/s41598-020-64246-3.

[47] N. R. Draper and H. Smith, *Applied Regression Analysis*, 3rd ed. John Wiley & Sons, Inc, 2014.

[48] N. Haandbæk, S. C. Bürgel, F. Rudolf, F. Heer, and A. Hierlemann, "Characterization of Single Yeast Cell Phenotypes Using Microfluidic Impedance Cytometry and Optical Imaging," *ACS Sens*, vol. 1, no. 8, pp. 1020–1027, 2016, doi: 10.1021/acssensors.6b00286.

[49] R. Reale, A. De Ninno, L. Businaro, P. Bisegna, and F. Caselli, "High-throughput electrical position detection of single flowing particles/cells with non-spherical shape," *Lab Chip*, vol. 19, no. 10, pp. 1818–1827, 2019, doi: 10.1039/C9LC00071B.

[50] D. Spencer and H. Morgan, "High-Speed Single-Cell Dielectric Spectroscopy," *ACS Sensors*, vol. 5, no. 2, pp. 423–430, 2020, doi: 10.1021/acssensors.9b02119.

[51] C. Honrado, L. Ciuffreda, D. Spencer, L. Ranford-Cartwright, and H. Morgan, "Dielectric characterization of Plasmodium falciparum-infected red blood cells using microfluidic impedance cytometry," *J. R. Soc. Interface*, vol. 15, no. 147, p. 20180416, Oct. 2018, doi: 10.1098/rsif.2018.0416.

[52] V. L. Sukhorukov, R. Benkert, G. Obermeyer, F. W. Bentrup, and U. Zimmermann, "Electrorotation of isolated generative and vegetative cells, and of intact pollen grains of Lilium longiflorum," *J. Membr. Biol.*,

vol. 161, no. 1, pp. 21–32, 1998, doi: 10.1007/s002329900311.

[53] K. Ahuja *et al.*, "Toward point-of-care assessment of patient response: a portable tool for rapidly assessing cancer drug efficacy using multifrequency impedance cytometry and supervised machine learning," *Microsystems Nanoeng.*, vol. 5, no. 1, p. 34, 2019, doi: 10.1038/s41378-019-0073-2.

[54] D. Yang, Y. Zhou, Y. Zhou, J. Han, and Y. Ai, "Biophysical phenotyping of single cells using a differential multiconstriction microfluidic device with self-aligned 3D electrodes," *Biosens. Bioelectron.*, vol. 133, pp. 16–23, 2019, doi: 10.1016/j.bios.2019.03.002.

[55] V. Sevillano, K. Holt, and J. L. Aznarte, "Precise automatic classification of 46 different pollen types with convolutional neural networks," *PLoS One*, vol. 15, no. 6, p. e0229751, 2020, doi: 10.1371/journal.pone.0229751.

[56] A. Kleiber, A. Ramoji, G. Mayer, U. Neugebauer, J. Popp, and T. Henkel, "3-Step flow focusing enables multidirectional imaging of bioparticles for imaging flow cytometry," *Lab Chip*, vol. 20, no. 9, pp. 1676–1686, 2020, doi: 10.1039/d0lc00244e.

[57] F. Caselli, A. De Ninno, R. Reale, L. Businaro, and P. Bisegna, "A Bayesian Approach for Coincidence Resolution in Microfluidic Impedance Cytometry," *IEEE Trans Biomed Eng*, vol. 68, no. 1, pp. 340–349, 2020, doi: 10.1109/TBME.2020.2995364.

[58] C. Honrado, J. S. McGrath, R. Reale, P. Bisegna, N. S. Swami, and F. Caselli, "A neural network approach for real-time particle/cell characterization in microfluidic impedance cytometry," *Anal. Bioanal. Chem.*, vol. 412, no. 16, pp. 3835–3845, 2020, doi: 10.1007/s00216-020-02497-9.

[59] X. Ren, P. Ghassemi, J. S. J. S. Strobl, and M. Agah, "Biophysical phenotyping of cells via impedance spectroscopy in parallel cyclic deformability channels," *Biomicrofluidics*, vol. 13, no. 4, p. 044103, 2019, doi: 10.1063/1.5099269.

[60] E. Katifori, S. Alben, E. Cerda, D. R. Nelson, and J. Dumais, "Foldable structures and the natural design of pollen grains," *Proc. Natl. Acad. Sci. U. S. A.*, vol. 107, no. 17, pp. 7635–7639, 2010, doi: 10.1073/pnas.0911223107.

[61] T. F. Fan *et al.*, "Transformation of hard pollen into soft matter," *Nat. Commun.*, vol. 11, no. 1, p. 1449, 2020, doi: 10.1038/s41467-020-15294-w.

[62] E. Martinelli, G. Magna, A. Vergara, and C. Di Natale, "Cooperative classifiers for reconfigurable sensor arrays," *Sens. Actuator B-Chem.*, vol. 199, pp. 83–92, 2014, doi: 10.1016/j.snb.2014.03.070.

[63] E. Hüllermeier and S. Vanderlooy, "Combining predictions in pairwise classification: An optimal adaptive voting strategy and its relation to weighted voting," *Pattern Recognit.*, vol. 43, no. 1, pp. 128–142, 2010, doi: 10.1016/j.patcog.2009.06.013.

[64] M. Polling *et al.*, "Neural networks for increased accuracy of allergenic pollen monitoring," *Sci. Rep.*, vol. 11, no. 1, 2021, doi: 10.1038/s41598-021-90433-x.

[65] F. Sedghy, A. R. Varasteh, M. Sankian, and M. Moghadam, "Interaction between air pollutants and pollen grains: The role on the rising trend in allergy," *Reports of Biochemistry and Molecular Biology*, vol. 6, no. 2. pp. 219–224, 2018.

[66] K. C. M. Lee, J. Guck, K. Goda, and K. K. Tsia, "Toward deep biophysical cytometry: prospects and challenges," *Trends Biotechnol.*, 2021, doi: 10.1016/j.tibtech.2021.03.006.